Ohmic Brownian Oscillator Approach to Hole-Burning and Photon-Echo Spectroscopies

Mohamad Toutounji

College of Science, Department of Chemistry, United Arab Emirates University, Al-Ain, UAE

Received: February 25, 2002; In Final Form: June 18, 2002

The multimode Brownian oscillator (MBO) model has been at the forefront in interpreting the subsystem−bath interaction manifestations in optical spectroscopy for probing homogeneous structure of chromophores in crystals and amorphous solids. The spectroscopic consequences of employing the underdamped MBO model with Ohmic dissipation in linear absorption, photon-echo, and hole-burning data of chromophores in solid hosts at low temperatures are investigated. The zero-phonon line (ZPL) in homogeneous linear absorption spectrum, the slow-decay component (due to ZPL) in photon-echo signal, and the zero-phonon hole (ZPH) in hole-burned spectra in host molecular solids at low temperatures are usually resolved from the multiphonon-transitions structure. In the MBO model, the harmonic vibrations (Brownian oscillators) are linearly coupled to bath modes. This coupling, with Ohmic dissipation, results in a maximum contribution of the bath modes to the ZPL region. This contribution affects the width of the ZPL profile, which should only be determined by pure electronic dephasing as dictated by experiments. It is therefore important to study how the MBO model bath modes contribute to the ZPL, ZPH, and slow-decay component profiles. Analytical expressions for the linear absorption spectrum and width and Franck−Condon factor of the ZPL are derived. Homogeneous linear absorption spectra, two-pulse photon-echo, and hole-burning calculations are carried out with model systems of which the parameter values are typical for real systems. The MBO model ZPL, ZPH, and slow-decay component were not seen in linear absorption, hole-burning, and two-pulse photon-echo profiles, respectively. The hole-burned spectrum is produced by blending the line broadening function, $g(t;T)$, of the MBO model and Small hole-burning formula. This full (inclusion of Matsubara series) form of $g(t;T)$ has not been exploited before in any spectroscopic calculation. It is concluded that the MBO model ZPL and ZPH widths and the electronic exponential decay are better exhibited in the corresponding profiles when using non-Ohmic spectral density.

I. Introduction

The recent advances in ultrafast spectroscopy performed with femtosecond laser pulses have made it possible to directly probe the electronic dephasing of solute chromophores in various hosts as a function of temperature.[1−7] This dephasing is caused by intermolecular vibrations (phonons) being coupled to the electronic transition of the chromophores. This coupling gives rise to the zero-phonon line (ZPL) and the phonon sideband (PSB) in the homogeneous line shape function. Hole-burning and photon-echo techniques have been used to study pure electronic dephasing of chromophores in glasses and polymers at low temperatures. Above about 15 K, the pure electronic dephasing is dominated by quadratic electron−phonon coupling, which gives rise to exchange coupling, for chromophores in host crystals. Linear optical experiments cannot extract the structural and dynamical information about molecular systems in condensed phases because they are usually hidden underneath a broad inhomogeneous distribution due to a variation in transition frequencies for different molecules as a result of different local environments. This is a typical linear spectrum in solutions, liquids, glasses, proteins, polymers, and molecular crystals. However, nonlinear optical techniques such as hole-burning, fluorescence line-narrowing, photon-echo, and pump−probe absorption can extract this information by eliminating the inhomogeneous broadening. Those techniques require going to higher-order optical response functions, that is, nonlinear response functions.[8]

The structural and dynamical information obtained from time domain measurements can be, equivalently, obtained from frequency domain experiments. For example, linear absorption and hole-burning line shapes in frequency domain and photon echo in time domain are due to the same electron−phonon coupling (which causes the same pure electronic dephasing), and therefore, they are related to each other: Fourier transform (FT) of a stimulated photon echo gives a hole-burning spectrum and Fourier cosine transform of accumulated photon echo yields a persistent hole-burning spectrum. Two-pulse photon echo (PE) is a powerful technique for measuring electronic dephasing, assuming no spectral diffusion, because FT of its decay gives the homogeneous optical line shape of the transition under study. In fact, PE decay measurements are linear absorption measurement hidden underneath a broad inhomogeneous distribution.[7,9−11] We recently derived a two-point dipole moment correlation function, $J(t;T)$, which enabled us to demonstrate that each component of the absorption line shape is related to the temporal behavior of the echo decay function over the relevant time scales.[7] For example, FT of the slow exponential decay in PE on the pico- and nanosecond time scales (slow-decay component) corresponds to the ZPL, while FT of nonexponential decay on the femtosecond time scales (ultrafast-decay component) corresponds to the PSB in the frequency domain. Finally, oscillations in time domain (quantum beats) correspond to Franck−Condon progressions in the frequency domain. Two-component photon-echo decays have been observed before by Saikan[10] and other workers,[5,10] for which the fast decay reflects

10.1021/jp025686r CCC: $22.00
Published on Web 09/06/2002

the PSB contribution and the slow one is due to the ZPL. It was shown that PE profile is a mirror image of linear absorption and hole-burning spectra.[7,10]

The multimode Brownian oscillator (MBO) model has gained a sound popularity in probing homogeneous structure of chromophores in liquids, molecular crystals, glasses, and polymers. It has been extremely important to the conceptual grasp of optical liquid dynamics[8,13−15] and ultrafast solvation dynamics.[8,13,16−19] In this model, the linearly coupled modes are the primary Brownian oscillators (BOs). The BOs and the bath modes (oscillators) are assumed to be harmonic with the coupling between the former and latter taken to be linear in the BO displacement, which results from excitation of the BO via the electronic transition. The coupling gives rise to an effective damping, $\gamma_j(\omega)$, for each BO, j (frequency, ω_j). In applications of the MBO model, the frequency dependence of γ_j has often been neglected, which amounts to a white spectrum for the bath (known as Ohmic dissipation). In the case of an underdamed Brownian oscillator, $\gamma_j < 2\omega_j$, this results in a ZPL width that depends on S_j, γ_j, and ω_j, where S_j is the Hung−Rhys factor and ω_j is the BO frequency. The spectroscopic consequences that arise upon applying the MBO model linear and nonlinear dipole moment correlation functions with Ohmic dissipation to low-temperature spectroscopy of chromophores imbedded in solids are that the contributions from decay of the excited state and pure electronic dephasing are neglected and that the ZPL width depends on S_j, γ_j, and ω_j.[6,20,21]

Another problem that arises in applying the model is that at sufficiently low temperatures the ZPL profile calculated by the MBO model with Ohmic dissipation was found to be *asymmetric*.[20,21] Single-molecule spectroscopy[22] and experiments of mixed organic crystals[23] and molecular chromophores in glasses and polymers[9,24−26] have shown that, for systems exhibiting weak electron−phonon coupling ($S < 1$), the ZPL profile is symmetric and that the width is determined by pure electronic dephasing (assuming no spectral diffusion).[1,2,20,21] Toutounji and Small[21] have examined in considerable detail the applicability of the Ohmic MBO model to linear optical spectroscopy of chromophores in host solids at low temperatures. They have formally proven, as we will see in section II, that the ZPL width vanishes at $T = 0$ K. The vanishing of the ZPL is clear evidence that the bath modes do not contribute to the ZPL line shape and that other dephasing mechanisms should be considered at low temperatures. As one raises the temperature, the ZPL starts acquiring finite width due to thermal activation of the bath modes. Knox et al.[20] have introduced non-Ohmic dissipation into the spectral density by using an empirical expression, whereby they were able to show that the inclusion of non-Ohmic dissipation, $\gamma_j(\omega)$, can lead to sharpening of the ZPL and a reduction in its asymmetry, depending on the magnitude of $\gamma_j(\omega)$. This is because non-Ohmic dissipation reduces the contribution from the bath modes to the ZPL profile, as should be the case.

Although the MBO model has been applied extensively to various spectroscopic techniques, solvation dynamics, electron transfer,[27] and energy transfer,[28] it has not yet been utilized in hole-burning spectroscopy. The only hole-burning theories that we are aware of are those of Personov,[9] Small and co-workers,[29] and Mukamel.[8] Here, we intend to blend the use of the line-broadening function, $g(t;T)$, which will include Matsubara frequencies, of the MBO model with the hole-burning formula of Small and co-workers.[29] Although the hole-burning theory of Small and co-workers has been designed to be implemented in frequency domain, in section IIB, we show that one can start from time domain through the use of $g(t;T)$ of the MBO model. In the case of Mukamel's formalism, a key quantity that enters into the MBO expressions for the linear and nonlinear response functions is the broadening function, $g(t;T)$, which depends on S_j, ω_j, and γ_j of the BOs. It was pointed out[6] in our previous work that $g(t;T)$ of the strongly underdamped MBO model leads to a ZPL width of $2S_j(2\bar{n}_j + 1)\gamma_j$, where $\bar{n}_j$ is the thermal oscillator of BO j and only when the frequency dependence of γ_j (non-Ohmic dissipation) is properly taken into account does $\gamma_j(\omega)$ vanish as $\omega \rightarrow 0$ so that bath modes do not contribute to the width of the ZPL. Inclusion of non-Markovian bath should rid the absorption in the ZPL region of the bath modes contribution. Thus, other dephasing mechanisms can dominate. Work in this direction is in progress.

In this paper, we intend to show the inadequacy of the Ohmic damping assumption when employing the MBO model to calculate linear/nonlinear spectra. The primary goal of carrying out photon-echo and hole-burning experiments is to study pure electronic dephasing. In section IIB, we show that the ZPL width dependence on S_j, ω_j, and γ_j of the BO could lead to erroneous conclusions about electronic dephasing data obtained from hole-burning and photon echo. A physical $g(t;T)$ that accounts for pure electronic dephasing has been proposed by Toutounji et al.[6,7] While this $g(t;T)$ is valid at any temperature, it is only good in the underdamped regime. There has been a considerable activity in applying the MBO model analysis to time-resolved spectroscopic techniques.[8,13−19,30−37] The difference between this paper and the alluded work is that this paper uses $g(t;T)$, which includes Matsubara series at finite temperatures in the underdamped regime, while the other groups had often used the overdamped MBO model $g(t;T)$ in the high-temperature limit.[12−14,16,17,19,30−37]

II. The Multimode Brownian Oscillator Model

In the MBO model, the quantum subsystem is taken to be a two electronic-level system with a ground state $|g\rangle$ and excited state $|f\rangle$ with some primary vibrational coordinates q_j (nuclear modes with angular frequency ω_j as part of the quantum subsystem) linearly coupled to the electronic system:

$$H = H_g|g\rangle\langle g| + H_f|f\rangle\langle f| + H' \tag{2.1}$$

where the nuclear Hamiltonians H_g and H_f are given by

$$H_g = \sum_j \left[\frac{p_j^2}{2m_j} + \frac{1}{2}m_j\omega_j^2 q_j^2\right] \tag{2.1a}$$

$$H_f = \sum_j \left[\frac{p_j^2}{2m_j} + \frac{1}{2}m_j\omega_j^2 (q_j + d_j)^2\right] \tag{2.1b}$$

and

$$H' = \sum_n \left[\frac{p_n^2}{2m_n} + \frac{1}{2}m_n\omega_n^2\left(Q_n - \sum_j \frac{c_{nj}q_j}{m_n\omega_n^2}\right)^2\right] \tag{2.1c}$$

The primary vibrational degrees of freedom are in turn linearly coupled to a harmonic bath made up of a set of oscillators with masses m_n, frequencies ω_n, coordinates Q_n (bath modes), and momenta p_n. The primary vibrational degrees of freedom (Brownian oscillators (BOs)) are coupled to the nth harmonic oscillator through the coupling strength c_{nj}. d_j is the linear displacement of the excited BO, which takes place upon optical

electronic transition. H' represents the bath oscillators and their coupling to the primary oscillators (phonons in solids) with a coupling strength c_{nj}.

A. Linear Spectroscopy. With the use of the Brownian oscillator model spectral density,[8] the linear dipole moment time correlation function, $J_{\mathrm{MBO}}(t;T)$, reads

$$J_{\mathrm{MBO}}(t;T) = \exp[-g(t;T) - i\Omega_{\mathrm{v}}t] \tag{2.2}$$

with $g(t;T) = \sum_{j=1}^{N} g_j(t;T)$ for a multimode (N Brownian oscillators (BOs)) system, and Ω_{v} is the vertical transition frequency. The line broadening function $g_j(t;T)$ for the jth BO is given by[23]

$$g_j(t;T) = F + \frac{S_j[-4i\varpi_j\gamma_j(\mathrm{e}^{-i\beta\hbar\gamma_j/2} - \cosh(\beta\hbar\varpi_j)) + (4\varpi_j^2 - \gamma_j^2)\sinh(\beta\hbar\varpi_j)]}{4\varpi_j\omega_j[\cos(\beta\hbar\gamma_j/2) - \cosh(\beta\hbar\varpi_j)]\,\mathrm{e}^{\gamma_j t/2}} \times \cos(\varpi_j t) + \frac{S_j[i(4\varpi_j^2 - \gamma_j^2)(\mathrm{e}^{-i\beta\hbar\gamma_j/2} - \cosh(\beta\hbar\varpi_j)) + 4\varpi_j\gamma_j\sinh(\beta\hbar\varpi_j)]}{4\varpi_j\omega_j[\cos(\beta\hbar\gamma_j/2) - \cosh(\beta\hbar\varpi_j)]\,\mathrm{e}^{\gamma_j t/2}} \times \sin(\varpi_j t) - \frac{2\gamma_j u_j^2}{\beta}\sum_{n=1}\frac{t - \nu_n^{-1}(1 - \mathrm{e}^{-\nu_n t})}{(\omega_j^2 + \nu_n^2)^2 - (\gamma_j\nu_n)^2} \tag{2.3}$$

$$F \equiv iS_j\gamma_j/\omega_j + b_1 + b_2 t \tag{2.3a}$$

$$b_1 \equiv \frac{S_j[4\varpi_j\gamma_j\sin(\beta\hbar\gamma_j/2) + (\gamma_j^2 - 4\varpi_j^2)\sinh(\beta\hbar\varpi_j)]}{4\varpi_j\omega_j[\cos(\beta\hbar\gamma_j/2) - \cosh(\beta\hbar\varpi_j)]} \tag{2.3b}$$

$$b_2 \equiv \frac{S_j\omega_j}{2}\,\frac{2\sin(\beta\hbar\gamma_j) + (\gamma_j/\varpi_j)\sinh(\beta\hbar\varpi_j)}{\cosh(\beta\hbar\varpi_j) - \cos(\beta\hbar\gamma_j/2)} \tag{2.3c}$$

In the above, we have introduced the positive bosonic Matsubara frequencies, $\nu_n = 2\pi n/(\beta\hbar)$, the Huang−Rhys factor, S_j, $u_j = \omega_j^{3/2}\bar{d}_j/\hbar^{1/2}$ where $\bar{d}_j$ is the dimensionless linear displacement, $\beta = (kT)^{-1}$ and T is the temperature, and $\varpi_j = (\omega_j^2 - \gamma_j^2)^{1/2}$ with γ_j and ω_j being the vibrational damping constant and fundamental angular frequency of the BO j (nuclear mode), respectively. The linear absorption spectrum can be obtained by taking the Fourier transform (FT) of $J_{\mathrm{MBO}}(t;T)$

$$\sigma_j(\omega;T) = \frac{\mathrm{Re}}{\pi}\int_0^\infty \mathrm{d}t\, J(t;T)\exp(i\omega t) \tag{2.4}$$

The result is derived in the Appendix A. The homogeneous width (fwhm) of the ZPL

$$\gamma_{\mathrm{ZPL},j}(T) = S_j\omega_j\frac{2\sin(\beta\hbar\gamma_j) + (\gamma_j/\varpi_j)\sinh(\beta\hbar\varpi_j)}{\cosh(\beta\hbar\varpi_j) - \cos(\beta\hbar\gamma_j/2)} - \sum_{n=1}^{\infty}\frac{4\gamma_j u_j^2/\beta}{(\omega_j^2 + \nu_n^2)^2 - (\gamma_j\nu_n)^2} \tag{2.5}$$

This width depends on S_j, ϖ_j, and γ_j. Equation 2.5 is an unphysical result; experimental studies and single-molecule spectroscopy show that the homogeneous ZPL width is due to pure electronic dephasing/spectral diffusion, see Introduction. Figure 1 shows homogeneous absorption spectra ($\omega_j = 30$ cm^{-1}, $\gamma_j = 20$ cm^{-1}, and $S_j = 1.8$ at $T = 15$ K) calculated using four values of the vibrational damping constant γ_j: 5, 10, 15, and 20 cm^{-1}. One can evidently see that the ZPL broadens significantly as γ_j increases yielding the following calculated, and measured, widths (eq 2.5): 12.5, 25, 37.6, and 50 cm^{-1}. Figure 1 was calculated by using eq 2.2 into eq 2.4. The bottom right frame corresponds to one of the modes of the special pair of bacterial reaction center.[38] The ZPL width in the absorption spectrum in the bottom right frame is in complete disagreement with that reported by experiment,[38] as well as with the theories of Small and co-workers[29,38] and Toutounji et al.[6,7] The experiment and the aforementioned theories distinctly show that the ZPL for the above parameters is Franck−Condon-allowed (the ZPL is resolved from the phonon-sideband structure), whereas Figure 1 shows otherwise. Figure 2 shows that the ZPL width depends on S_j. Changing from $S_j = 1.8$ used in Figure 1 (upper left frame) to $S_j = 4$, and keeping everything else fixed, yields Figure 2 with a ZPL width of 27.8 cm^{-1}. For a small magnitude of γ_j, Ohmic dissipation leads to a ZPL width that is too large, that is, unphysical. Equation 2.5 was used to accurately reproduce the results given in Figure 2 of ref 20.

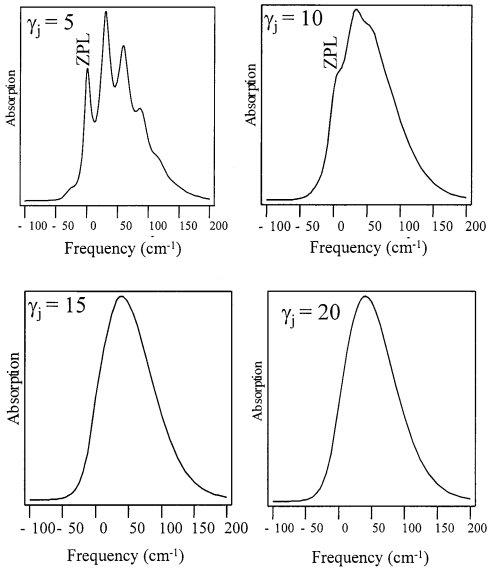

Figure 1. Homogeneous linear absorption spectra calculated with numerical Fourier transform of $J_{\mathrm{MBO}}(t;T)$ for a model system at various vibrational dampings γ_j: $\omega_j = 30$ cm^{-1}, $S_j = 1.8$, and $T = 15$ K. It is clearly shown how the ZPL width and intensity change as a function of γ_j. This is an artifact of the MBO model. The bottom right frame with $\gamma_j = 20$ cm^{-1} represents the 30 cm^{-1} mode for the special pair absorption band of the bacterial reaction center.

Note that eq 2.5 reduces to zero at $T = 0$, vide infra. The homogeneous widths of the multiphonon bands are given by[6,21]

$$(\mathrm{fwhm})_k = \gamma_{\mathrm{ZPL},j} + |k|\gamma_j \tag{2.6}$$

k is an integer that signifies the number of phonons created/annihilated with each vibronic transition. That $\gamma_{\mathrm{ZPL},j}$ adds to the widths of the multiphonon transition has a physical basis.[39] The linear dependence on k (folding) is valid for any phonon relaxation mechanism that is linear in the coordinate

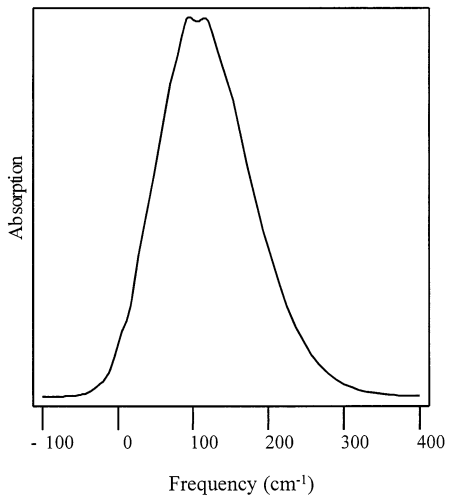

Figure 2. Homogeneous linear absorption spectrum calculated with numerical Fourier transform of $J_{MBO}(t;T)$ for a model system: $\omega_j = 30$ cm^{-1}; $\gamma_j = 5$ cm^{-1}; $S_j = 4$, and $T = 15$ K. This figure shows how changing S_j from 1.8 in Figure 1 to 4 affects the entire spectral profile starting with that of the ZPL.

of the phonon. Such folding has been observed for chromophores in host crystals.[39,40] The FC factor for the ZPL is (see Appendix A)

$$FC_{ZPL,j} = \exp\left\{-iS_j\gamma_j/\omega_j - \Sigma_j - \sum_{n=1}^{\infty} \frac{2\gamma_j u_j^2/(\beta\nu_n)}{(\omega_j^2 + \nu_n^2)^2 - (\gamma_j\nu_n)^2}\right\} \quad (2.7)$$

where

$$\Sigma_j \equiv \frac{S_j[4\varpi_j\gamma_j \sin(\beta\hbar\gamma_j/2) + (\gamma_j^2 - 4\varpi_j^2)\sinh(\beta\hbar\varpi_j)]}{4\varpi_j\omega_j[\cos(\beta\hbar\gamma_j/2) - \cosh(\beta\hbar\varpi_j)]} \quad (2.8)$$

Equation 2.8 recovers the well-known form, $FC_{ZPL,j} = \exp[-S_j \coth(\beta\hbar\omega_j/2)]$ as $\gamma_j \rightarrow 0$.

The linear dipole moment correlation function $J_{MBO}(t)$, for BO j at $T = 0$ K is given by (see Appendix B)

$$J_{MBO}(t) = \exp\{-Y_j(1 - \exp(-\gamma_j t/2 - i\varpi_j t)) + D_j\} \quad (2.9)$$

where

$$Y_j \equiv S_j\left(\omega_j^2 - \frac{\gamma_j^2}{2} + i\gamma_j\varpi_j\right)/\varpi_j\omega_j \quad (2.9a)$$

and

$$D_j \equiv -\frac{\omega_j^3 d_j^2 \gamma_j}{\pi}\int_0^{\infty} \frac{dx\, x^{-1}(1 - e^{-xt})}{(\omega_j^2 + x^2)^2 - (\gamma_j x)^2} \quad (2.9b)$$

See ref 21 for the mathematical behavior of D_j. The absorption line shape my be obtained by using eq 2.9 in eq 2.4 to give[21]

$$\sigma_{MBOj}(\omega) = \frac{\mathrm{Re}}{\pi}\left\{\exp(-Y_j)\sum_{m=0}^{\infty}\frac{Y_j^m}{m!}\left[\frac{(m\gamma_j/2) + i(\omega - m\varpi_j)}{(\omega - m\varpi_j)^2 + (m\gamma_j/2)^2}\right]\right\} * f_j(\omega) \quad (2.10)$$

where $f_j(\omega)$ is the Fourier transform of $\exp(D_j)$ and "$*$" denotes convolution.

Note that the time-dependent part of $\exp(D_j)$ or the frequency dependence of its Fourier transform $f_j(\omega)$ contribute only to the vibrational (phonons) part of the absorption spectrum. Thus, the frequency-independent term in $f_j(\omega)$ would contribute only to the FC factor of the ZPL. Because we are in the low-temperature limit, the quantum number of the initial state for the absorption transition is zero. m is the final-state quantum number. Equation 2.10 shows, in part, that MBO model yields a ZPL ($m = 0$) homogeneous width of zero. The homogeneous widths (fwhm) of the multiphonon bands ($m \geq 1$) are $m\gamma_j$. Note, however, that this gives folding to the widths of the multiphonon transitions, which will often be the desired result. Equation 2.10 shows that the ZPL blows up[21] at $T = 0$. The presence of zero width of the ZPL, that is, delta-function line shape, in eq 2.10 has a great spectroscopic advantage in the sense that one can feed in the correct pure electronic dephasing function, as was done in refs 6 and 21, because the MBO model neglects it. It further indicates that the bath modes do not contribute to the ZPL line shape at $T = 0$ K. It is interesting to note that in reference to eq 2.10 one obtains the familiar Poisson distribution $\exp(-S_j)\sum_m(S_j^m/m!)$ for FC factors in the limit $\gamma_j \rightarrow 0$ with $\varpi_j \rightarrow \omega_j$.

B. Nonlinear Spectroscopy. Consider the impulsive stimulated photon echo in which the three applied pulses are infinitely short. The integrated intensity of the echo signal, S_{SPE}, is[8]

$$S_{SPE}(\tau',\tau) = \int_0^{\infty} dt\, |\mathbf{R}(t,\tau,\tau')|^2 |\chi(t - \tau')|^2 \quad (2.11)$$

where τ' is the delay between the first and second pulses and τ is the delay between the second and third pulses. Here, $\mathbf{R}(t_3,t_2,t_1)$ is the echo response function defined as[8]

$$\mathbf{R}(t_3,t_2,t_1) \equiv R_2(t_3,t_2,t_1) + R_3(t_3,t_2,t_1) \quad (2.12)$$

where $R_2(t_3,t_2,t_1)$ and $R_3(t_3,t_2,t_1)$ can be found in ref 8. While $\mathbf{R}(t_3,t_2,t_1)$ governs the homogeneous (dynamical) contribution to the dephasing, $\chi(t_3 - t_1)$ governs the static inhomogeneous contribution. The form of the inhomogeneous broadening term χ, vide infra, results in the maximum of the echo appearing at time $t = \tau'$ after the interaction with the third pulse, which we can now consider to have occurred at $t = 0$. For $t > \tau'$, the echo decays because of dephasing. If in the frequency domain the inhomogeneous broadening is far greater than the homogeneous broadening, $\chi(t - \tau')$ in eq 2.11 can be approximated by a delta function, which results in

$$S_{SPE}(\tau',\tau) = |\mathscr{R}(\tau',\tau,\tau')|^2 \quad (2.13)$$

In the calculations that follow a Gaussian profile is used for the inhomogeneous function χ:

$$\chi(t_3 - t_1) = \exp\left[-\frac{1}{2}w^2(t_3 - t_1)^2\right] \quad (2.14)$$

where the parameter w is related to the fwhm of the inhomogeneous profile in the frequency domain by fwhm $= 2.35w$.

The impulsive two-pulse echo (IPE) can be calculated by setting $\tau = 0$ in eq 2.11. Using the echo response function, $\mathbf{R}(\tau',0,\tau')$, in eq 2.11 yields the integrated impulsive two-pulse echo signal, $S_{IPE}(\tau';T)$:

$$S_{IPE}(\tau';T) = \int_0^{\infty} dt \exp[-w^2(t - \tau')^2] \exp\{-2\,\mathrm{Re}[2g(t;T) + 2g(\tau';T) - g(t + \tau';T)]\} \quad (2.15)$$

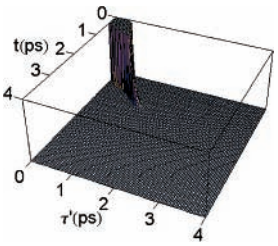

Figure 3. The 3-D graph is the IPE signal as a function of t and τ' calculated with eq 2.16 employing the same parameters used in the bottom right frame of Figure 1. The fast nonexponential decay signifies the PSB. The slow-decay component (ZPL) is not present; see text for details.

The time-resolved two-pulse echo is

$$S_{\mathrm{IPE}}(t,\tau';T) = \exp[-w^2(t-\tau')^2]\exp\{-2\,\mathrm{Re}[2g(t;T) + 2g(\tau';T) - g(t+\tau';T)]\} \quad (2.16)$$

Figure 3 is a direct application of eq 2.16 for the same parameters used in Figure 1 with $\gamma_j = 20$ cm^{-1} and $w = 64$ cm^{-1}. The 3-D graph shows the behavior of the echo along the $t = \tau'$ diagonal. Following the initial fast nonexponential (free-induction) decay of the intense PSB features associated with the overall profile of the multiphonon transitions, one would expect to observe a fundamental quantum beat at 1.1 ps and its overtone at 2.2 ps, as was observed in ref 7. Although the ZPL[7] is expected to be present (Franck−Condon allowed), the slow-decay component is not observed in Figure 3. This disparity is attributed to the contribution from the bath modes to the slow-decay component (dependence of the ZPL width on S_j, γ_j, and ω_j), which makes the ZPL Franck−Condon-forbidden and thus not reflected in the PE profile. PE features in Figure 3 are in disagreement with the PE results of ref 7 (PE results of ref 7 are in good agreement with experiment, as well as with Small theory). Clearly, the structurelessness (lack of beats and the ZPL) of the homogeneous absorption spectrum in Figure 1 is noticeably manifested in Figure 3. Equation 2.15 is effectively the projection of the echo surface, produced by eq 2.16, along the time-delay axis. The integrated intensity calculation was performed, and the results (not shown) confirmed the findings of Figure 3.

We now use $J_{\mathrm{MBO}}(t;T)$ in the hole-burning theory of Small and co-workers[29] to calculate the hole-burned spectrum for one mode of the special pair absorption band of the bacterial reaction center. The absorption spectrum following a burn for time η is given by[38−40]

$$\sigma_\eta(\omega;T) = \int_{-\infty}^{+\infty} \mathrm{d}\Omega\, \chi(\Omega-\nu_m) J_{\mathrm{MBO}}(\omega-\Omega;T)\exp[-\rho J_{\mathrm{MBO}}(\omega_{\mathrm{B}}-\Omega;T)\eta] \quad (2.17)$$

where Ω is the frequency of the ZPL of a single absorber and ω_{B} is the burn frequency. $\chi(\Omega - \nu_m)$ is a Gaussian function with variance w^2 centered at ν_m, which governs the distribution of ZPL frequencies due to structural heterogeneity. ρ is the product of three terms: the absorption cross-section, the laser burn flux, and the quantum yield for hole-burning. $J_{\mathrm{MBO}}(\omega - \Omega;T)$ is the absorption spectrum of a single site of which the ZPL frequency is Ω. Note that for $\eta = 0$, eq 2.17 is the inhomogeneously broadened absorption spectrum. The hole-burned spectrum is defined here as $\sigma_\eta(\omega;T) - \sigma_0(\omega;T)$. The value for the standard deviation of $\chi(\Omega - \nu_m)$ used was 64 cm^{-1} [38] (ν_m was set equal to zero with ω_{B} set equal to ν_m). ρ_η was set at 0.004. Using the MBO model $g(t)$ at $T = 0$ K poses a numerical problem, because the ZPL line shape becomes a delta function, according to eq 2.10, but that one can be avoided by introducing pure electronic dephasing.[6,21] The 15 K hole-burned spectrum of Figure 4 disagrees with the experimental spectrum[32] (although the experiment was conducted on a two-mode system, the ZPL result should be the same because the ZPL profile is insensitive to vibrational structure), as well as the spectrum calculated using the frequency domain theory of Small and co-workers[6] (not shown). Note the very weak intensity of the zero-phonon hole (ZPH) at ω_{B}, which carries a width of $2\gamma_{\mathrm{ZPL}} = 100$ cm^{-1} (this width is orders of magnitude larger than that experimentally observed one. The weakness of the ZPH can be understood from its unphysically large width). The Franck−Condon progressions are also lost because the ZPH width extends to the vibrational structure. The underdamped mode is acting as if it were an overdamped mode. This, again, is due to the maximal contribution from the bath modes to the ZPH profile.

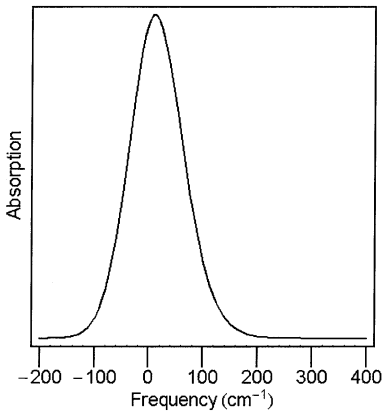

Figure 4. Hole-burned spectrum for the 30 cm^{-1} mode of the special pair absorption band of the bacterial reaction center calculated with eq 2.17 using the same parameters given in the Figure 3 caption. The ZPH is missing; see text for details.

Another example that illustrates the inadequacy of the Ohmic assumption when using the MBO model is the model system with $S_j = 0.3$, $\gamma_j = 10$ cm^{-1}, and $\omega_j = 25$ cm^{-1} at $T = 15$, 25, and 100 K. (This system, which quite closely mimics Al-phthalocyanine tetrasulfonate in glassy ethanol,[2] exhibits weak electron−phonon coupling ($S < 1$), in contrast to the earlier example, which showed strong electron−phonon coupling.) The MBO ZPH widths at the alluded temperatures, respectively, are 10, 16.7, and 66 cm^{-1}, whereas the corresponding reported widths[7] are 0.14, 1.0, and 15.2 cm^{-1}. The phonon-sideband hole widths will in turn be significantly larger than those reported in refs 2 and 7.

The problem of unphysically large ZPH width in hole-burning extends to the widths of the vibrational progressions because they build on the ZPL width. Similarly, the problem of the too fast electronic exponential decay in photon echo merges with the femtosecond time scale of the quantum beats (nonexponential decay) and thus leads to significant errors on interpreting the experimental data.

III. Conclusions

This paper is the result of calculations that were carried out in applying the MBO model to understanding the relationship and differences between optical coherence loss of a chromophore in a glass and in the liquid phase of the glass-forming solvent. We offered first-time work in which the exact line broadening

function $g(t;T)$ (eq 2.3) is used in nonlinear spectroscopy. As extensive numerical calculations were being performed to obtain linear and nonlinear spectra, the MBO model ZPL measurements showed noticeable disagreement with those of the experimental results and with well-established theories as well, especially when these theories agree with experiment. We believe that this disagreement is attributed to using Ohmic spectral density in the MBO model. Using Ohmic dissipation gave rise to difficulties, namely, asymmetric ZPL and its width dependence on the vibrational parameters such as S_j, γ_j, and ω_j. Experimental studies show that homogeneous ZPL width is due to electronic dephasing in which vibrational parameters have no role. While the multiphonon transitions widths should build on the ZPL width, the Ohmic MBO model indicates the converse.

The primary goal of carrying out photon-echo and hole-burning experiments is to study pure electronic dephasing through analyzing and quantifying the slow exponential decay and ZPH width. The ZPL, ZPH, and slow electronic exponential decay in homogeneous linear absorption, hole-burning, and two-pulse photon-echo profiles were missing when applying the Ohmic MBO model to the special pair of the bacterial reaction center. The absence of theses three profiles was ascribed to the dependence of the electronic transition on S_j, γ_j and ω_j. This dependence is caused by the bath modes contributing to the ZPL region. This contribution is attributed to using Ohmic spectral density in formulating the MBO model. Thus, the use of the Ohmic MBO model to interpret data on relaxation dynamics of active BOs can lead to incorrect conclusions. The MBO model problem may be solved by introducing non-Ohmic dissipation, which will in turn lead to a dipole moment correlation function with a ZPL width of zero. One can then add in an electronic correlation function that accounts correctly for pure electronic dephasing, as was done in refs 6 and 21.

It should be pointed out that our remarks in this article do not constitute the failure or deficiency of the MBO model. They are, however, to propose to the MBO model user to practice care when applying the MBO model with Ohmic dissipation. Redfield theory and the MBO model are perhaps the most widely used relaxation models. Recently, there have been some theoretical studies in electron-transfer dynamics favoring the semigroup analysis over Redfield theory[41] because of the positive dynamics that the semigroup approach[42−45] can ensure and that Redfield theory fails to warrant. The reason that the Redfield approach does not warrant positive dynamics, as pointed out by the Silbey group,[46] is that the Markovian assumption would not hold unless nonlocal memory effects take place in a very short time scale. It is only after this transient time that the subsystem dynamics are properly described by the Markovian regime, which is equivalent to Ohmic dissipation. Just because the Redfield theory does not warrant positivity, this does not constitute its failure. It does however signal that the Markovian approximation in some cases may produce nonpositive dynamics. Similarly, the asymmetry of the MBO model and its ZPL width dependence on the model vibrational parameters do not constitute its failure. It does nonetheless suggest introducing non-Ohmic dissipation into the spectral density of the phonons. Non-Ohmic damping (non-Markovian relaxation) implies noninstantaneous dissipation, which allows transient correlations between the subsystem and the bath to arise during the time and the subsystem being correlated. Ohmic damping does not offer this feature. However, it was found that the Ohmic MBO model can prove reasonably valid in the strongly underdamped regime, that is, $\gamma_j \ll 2\omega_j$.

Acknowledgment. The author would like to thank the United Arab Emirates University Research Council for funding this project, under the Limited Research Grant Scheme 2000/2001. I am specially thankful to Gerald J. Small for stimulating and useful discussions.

Appendix A

Here, we provide a derivation of the linear absorption spectrum line shape function, $\sigma_{\mathrm{MBO}_j}(\omega;T)$ at a finite temperature from which the FC factor and the ZPL homogeneous width can be obtained. The line broadening function $g_j(t;T)$ is given by[8]

$$g_j(t;T) = u_j^2 \int_0^t \mathrm{d}\tau_1 \int_0^{\tau_1} \mathrm{d}\tau_2\, C_j'(\tau_2) + i u_j^2 \int_0^t \mathrm{d}\tau_1 \int_0^{\tau_1} \mathrm{d}\tau_2\, C_j''(\tau_2) \tag{A1}$$

where $u_j = \omega_j^{3/2}\bar{d}_j/\hbar^{1/2}$and $\bar{d}_j$ is the dimensionless linear displacement. $C_j'(t)$ and $C_j''(t)$ are the real and imaginary parts of the two-time position correlation function $C_j(t;T)$ for underdamped ($\gamma_j < 2\omega_j$) BO j. They are given by

$$C_j'(t) = \frac{\hbar}{4\varpi_j}[\coth(i\phi_j'\hbar\beta/2)\,\mathrm{e}^{-\phi_j' t} - \coth(i\phi_j\hbar\beta/2)\,\mathrm{e}^{-\phi_j t}] - \frac{2\gamma_j}{\beta}\sum_{n=1}^{\infty}\frac{\nu_n\,\mathrm{e}^{-\nu_n t}}{(\omega_j^2+\nu_n^2)^2-(\gamma_j\nu_n)^2} \tag{A2}$$

$$C_j''(t) = -\frac{\hbar}{2\varpi_j}\sin(\varpi_j t)\,\mathrm{e}^{-\gamma_j t/2} \tag{A3}$$

where $\phi_j = \gamma_j/2 + i\varpi_j$ and $\phi_j' = \gamma_j/2 - i\varpi_j$. Carrying out the double integral in eq A1 yields

$$-g_j(t;T) = F + (a_1\cos(\varpi_j t) + a_2\sin(\varpi_j t))\,\mathrm{e}^{-\gamma_j t/2} + \frac{2\gamma_j u_j^2}{\beta}\sum_{n=1}\frac{t-\nu_n^{-1}(1-\mathrm{e}^{-\nu_n t})}{(\omega_j^2+\nu_n^2)^2-(\gamma_j\nu_n)^2} \tag{A4}$$

where

$$F \equiv -iS_j\gamma_j/\omega_j - b_1 - b_2 t \tag{A5}$$

$$a_1 \equiv \frac{S_j[-4i\varpi_j\gamma_j(\mathrm{e}^{-i\beta\hbar\gamma_j/2}-\cosh(\beta\hbar\varpi_j)) + (4\varpi_j^2-\gamma_j^2)\sinh(\beta\hbar\varpi_j)]}{\alpha} \tag{A6}$$

and

$$a_2 \equiv -\frac{S_j[i(4\varpi_j^2-\gamma_j^2)(\mathrm{e}^{-i\beta\hbar\gamma_j/2}-\cosh(\beta\hbar\varpi_j)) + 4\varpi_j\gamma_j\sinh(\beta\hbar\varpi_j)]}{\alpha} \tag{A7}$$

with

$$b_1 \equiv -\frac{S_j[4\varpi_j\gamma_j\sin(\beta\hbar\gamma_j/2) + (\gamma_j^2-4\varpi_j^2)\sinh(\beta\hbar\varpi_j)]}{\alpha} \tag{A8}$$

where $\alpha \equiv 4\varpi_j\omega_j(\cosh(\beta\hbar\varpi_j) - \cos(\beta\hbar\gamma_j/2))$ and

$$b_2 \equiv \frac{S_j\omega_j}{2}\frac{2\sin(\beta\hbar\gamma_j) + (\gamma_j/\varpi_j)\sinh(\beta\hbar\varpi_j)}{\cosh(\beta\hbar\varpi_j) - \cos(\beta\hbar\gamma_j/2)} \tag{A9}$$

One may rewrite $J_{MBO,j}(t;T)$ as ($\Omega = 0$)

$$J_{MBO,j}(t,T) = e^{F} \sum_{k=-\infty}^{\infty}\sum_{l=0}^{\infty}(Z_1/2)^{k+2l}\frac{\exp(ik\Theta_j)}{l!\Gamma(k+l+1)} \times \exp[-(b_2 - b_3 + (k+2l)\gamma_j/2)t] \times \exp(-ik\varpi_j t)\prod_{n=1}^{\infty}\sum_{m=0}^{\infty}\frac{(2u_j^2\gamma_j\beta^{-1}\nu_n^{-1})^m e^{-m\nu_n t}}{m!((\omega_j^2+\nu_n^2)^2-(\gamma_j\nu_n)^2)^m} \quad (A10)$$

where $Z_1 = \sqrt{a_1^2 + a_2^2}$ and $\Theta_j = \arctan(a_2/a_1)$. The linear absorption $\sigma_{MBO,j}(\omega;T)$ is given by

$$\sigma_{MBO,j}(\omega;T) = \frac{Re}{\pi}\int_0^{\infty} dt\, J_{MBO,j}(t;T)\exp(i\omega t) \quad (A11)$$

Applying eq A11 to eq A10 leads directly to

$$\sigma_{MBO,j}(\omega;T) = \frac{Re}{\pi} e^{-iS_j\gamma_j/(\omega_j - b_1 - b_4)}\sum_{k=-\infty}^{\infty}\sum_{l=0}^{\infty}\prod_{n=1}^{\infty}\sum_{m=0}^{\infty}(Z_1/2)^{k+2l} \times \frac{\exp(ik\Theta_j)(2u_j^2\gamma_j\beta^{-1}\nu_n^{-1})^m}{m!l!\Gamma(k+l+1)}((\omega_j^2+\nu_n^2)^2-(\gamma_j\nu_n)^2)^{-m} \times (b_2 - b_3 + (k+2l)\gamma_j/2 + m\nu_n + i(k\varpi_j - \omega))^{-1} \quad (A12)$$

where

$$b_3 = \sum_{n=1}^{\infty}\frac{2u_j^2\gamma_j\beta^{-1}}{(\omega_j^2+\nu_n^2)^2-(\gamma_j\nu_n)^2} \quad (A13)$$

and $b_4 = b_3/\nu_n$. Γ is the gamma function. Equation 2.7 and the homogeneous width of the ZPL in eq 2.5 can easily be obtained by setting $k = l = m = 0$, whereas the widths of the multiphonon transitions are given by eq 2.6.

Appendix B

In this appendix, we sketch the derivation of the MBO model linear dipole moment correlation function at $T = 0$ K. In the low-temperature limit, $C_j'(t)$ and $C_j''(t)$ (from Appendix A) read

$$C_j'(t) = \frac{\hbar}{2\varpi_j}\cos(\varpi_j t)\, e^{-\gamma_j t/2} - \lim_{\beta\to\infty}\frac{2\gamma_j}{\beta}\sum_{n=1}^{\infty}\frac{\nu_n e^{-\nu_n t}}{(\omega_j^2+\nu_n^2)^2-(\gamma_j\nu_n)^2} \quad (B1)$$

$$C_j''(t) = -\frac{\hbar}{2\varpi_j}\sin(\varpi_j t)\, e^{-\gamma_j t/2} \quad (B2)$$

As the temperature is lowered, quantum effects start to appear and the Matsubara frequencies ν_n get closer to each other, and at zero temperature, all of them contribute. One may then replace the Matsubara sum in eq B1 by an integral

$$-\lim_{\beta\to\infty}\frac{2\gamma_j}{\beta}\sum_{n=1}^{\infty}\frac{\nu_n e^{-\nu_n t}}{(\omega_j^2+\nu_n^2)^2-(\gamma_j\nu_n)^2} = -\frac{\hbar\gamma_j}{\pi}\int_0^{\infty} dx\,\frac{x e^{-xt}}{(\omega_j^2+x^2)^2-(\gamma_j x)^2} \quad (B3)$$

One can evaluate the $J_{MBO}(t;T)$ by substituting eq B3 in the real term of eq A1 and then exponentiating it as in eq 2.2. As a result, $C_j'(t)$ assumes this form

$$C_j' = \frac{\hbar}{2\varpi_j}\cos(\varpi_j t)\, e^{-\gamma_j t/2} - \frac{\hbar\gamma_j}{\pi}\int_0^{\infty} dx\,\frac{x e^{-xt}}{(\omega_j^2+x^2)^2-(\gamma_j x)^2} \quad (B4)$$

When eq B1 is used, $g_j(t)$ reads, at $T = 0$ K,

$$g_j(t) = S_j\omega_j\gamma_j t/(2\varpi_j) + Y_j(1 - \exp(-\gamma_j t/2 - i\varpi_j t)) - \frac{\omega_j^3\bar{d}_j^2\gamma_j}{\pi}\int_0^{\infty} dx\,\frac{t - x^{-1}(1 - e^{-xt})}{(\omega_j^2+x^2)^2-(\gamma_j x)^2} \quad (B5)$$

where

$$Y_j \equiv S_j\left(\omega_j^2 - \frac{\gamma_j^2}{2} + i\gamma_j\varpi_j\right)/(\varpi_j\omega_j) \quad (B6)$$

where $S_j = \bar{d}_j^2/2$ is the Huang−Rhys factor with $\bar{d}_j$ being the dimesionless linear displacement and γ_j is the damping constant (fwhm) of the jth BO. When eq 2.2 is utilized, $J_{MBO}(t)$ reads, for a single-mode system ($\Omega = 0$),

$$J_{MBO}(t) = \exp\left\{-S_j\omega_j\gamma_j t/(2\varpi_j) - Y_j(1 - \exp(-\gamma_j t/2 - i\varpi_j t)) + \frac{\omega_j^3\bar{d}_j^2\gamma_j}{\pi}\int_0^{\infty} dx\,\frac{t - x^{-1}(1 - e^{-xt})}{(\omega_j^2+x^2)^2-(\gamma_j x)^2}\right\} \quad (B7)$$

Equation B7 may be simplified through the fact that the first term in the integral multiplied by $\omega_j^3\bar{d}_j^2\gamma_j/\pi$ is equal to $S_j\omega_j\gamma_j/(2\varpi_j)$. $J_{MBO}(t)$ in turn becomes

$$J_{MBO}(t) = \exp\{-Y_j(1 - \exp(-\gamma_j t/2 - i\varpi_j t)) + D_j\} \quad (B8)$$

where

$$D_j \equiv -\frac{\omega_j^3\bar{d}_j^2\gamma_j}{\pi}\int_0^{\infty}\frac{dx\, x^{-1}(1 - e^{-xt})}{(\omega_j^2+x^2)^2-(\gamma_j x)^2} \quad (B9)$$

References and Notes

(1) Reinot, T.; Kim, W.-H.; Hayes, J. M.; Small, G. J. *J. Chem. Phys.* **1996**, *104*, 793.
(2) Reinot, T.; Kim, W.-H.; Hayes, J. M.; Small, G. J. *J. Chem. Phys.* **1997**, *106*, 457.
(3) Nagasawa, Y.; Passino, S. A.; Joo, T.; Fleming, G. R. *J. Chem. Phys.* **1997**, *106*, 4840.
(4) Bardeen, C. J.; Cerullo, G.; Shank, C. V. *Chem. Phys. Lett.* **1997**, *280*, 127.
(5) Schellenberg, P.; Louwe, R. J. W.; Shochat, S.; Gast, P.; Artsma, T. J. *J. Phys. Chem. B* **1997**, *101*, 6786.
(6) Toutounji, M.; Small, J. G.; Mukamel, S. *J. Chem. Phys.* **1998**, *109*, 7949.
(7) Toutounji, M.; Small, J. G.; Mukamel, S. *J. Chem. Phys.* **1999**, *110*, 1017.
(8) Mukamel, S. *Principles of Nonlinear Optical Spectroscopy*; Oxford University Press: New York, 1995.
(9) *Spectroscopy and Excitation Dynamics of Condensed Molecular Systems*; Agranovich, V. M., Hochstrasser, R. M., Eds.; North-Holland: Amsterdam, 1983.

(10) Saikan, S.; Nakabayashi, T.; Kanematsu, Y.; Tato, N. *Phys. Rev. B* **1988**, *38*, 7777. Saikan, S.; Imaoka, A.; Kanematsu, Y.; Sakoda, K.; Kominami, K.; Iwamoto, M. *Phys. Rev. B* **1990**, *41*, 3185. Saikan, S.; Kanematsu, Y.; Shiraishi, R.; Nakabayashi, T.; Kushida, T. *J. Lumin*. **1987**, *38*, 15. Saikan, S.; Lin, J. W.-I.; Nemoto, H. *Phys. Rev. B* **1992**, *46*, 11125.

(11) Asaka, S.; Nakatsuka, H.; Fujiwara, M.; Matsuka, M. *Phys. Rev. A* **1984**, *29*, 2286.

(12) Yan, Y. J.; Fried, L. E.; Mukamel, S. *J. Chem. Phys*. **1989**, *93*, 8149.

(13) Pshenichnikov, M. S.; Duppen, K.; Wiersma, D. A. *Phys. Rev. Lett*. **1995**, *74*, 674.

(14) Bosma, W. B.; Yan, Y.; Mukamel, S. *Phys. Rev. A* **1990**, *42*, 9620.

(15) McMorrow, D.; Lotshow, W. T. *Chem. Phys. Lett*. **1991**, *178*, 69. McMorrow, D.; Lotshow, W. T. *J. Chem. Phys*. **1991**, *95*, 1035.

(16) Mukamel, S. *Annu. Rev. Phys. Chem*. **1990**, *41*, 647; *Adv. Chem. Phys*. **1988**, *70*, 165.

(17) Bardeen, C. J.; Shank, C. V. *Chem. Phys. Lett*. **1994**, *310*, 226.

(18) Fleming, G. R.; Cho, M. *Annu. Rev. Phys. Chem*. **1996**, *47*, 109.

(19) de Boeij, W. P.; Pshenichnikov, M. S.; Wiersma, D. A. *J. Phys. Chem*. **1996**, *100*, 11806.

(20) Knox, R. S.; Small, G. J.; Mukamel, S. *Chem. Phys*., in press.

(21) Toutounji, M.; Small, G. J. *J. Chem. Phys.* **2002**, *117*, 3848.

(22) Kozankiewicz, B.; Bernard, J.; Orrit, M. *J. Chem. Phys*. **1994**, *101*, 9377 and references therein.

(23) Burke, P.; Small, G. J. *J. Chem. Phys.* **1974**, *5*, 198 and references therein.

(24) *Persistent Spectral Hole Burning: Science and Applications*; Moerner, W. E., Ed.; Springer: New York, 1987; Vol. 44.

(25) Liattu, K. A.; Fayer, M. D. *Chem. Phys. Lett*. **1991**, *176*, 551.

(26) van der Zaag, P. J.; Galaup, J. P.; Volker, S. *Chem. Phys. Lett*. **1990**, *166*, 263.

(27) Chernyak, V.; Wang, N.; Mukamel, S. *Phys. Status Solidi B* **1995**, *188*, 275.

(28) Mukamel, S.; Rupasov, V. *Chem. Phys. Lett*. **1995**, *242*, 17.

(29) Hayes, J. M.; Lyle, P. A.; Small, G. J. *J. Phys. Chem*. **1994**, *98*, 7337.

(30) Vöhringer, P.; Arnett, D. C.; Yang, T.-S.; Scherer, N. F. *Chem. Phys. Lett*. **1995**, *237*, 387.

(31) Joo, T.; Jia, Y.; Yu, J.-Y.; Lang, M. J.; Fleming, G. R. *J. Chem. Phys*. **1996**, *104*, 6089.

(32) Cruz, C. H. B.; Frork, R. L.; Knox, W. H.; Shank, C. V. *Chem. Phys. Lett*. **1986**, *132*, 341.

(33) de Boeij, W. P.; Pshenichnikov, M. S.; Duppen, K.; Wiersma, D. A. *Chem. Phys. Lett*. **1995**, *138*, 1.

(34) Yan, Y. J.; Mukamel, S. *J. Chem. Phys*. **1991**, *94*, 179.

(35) Yan, Y. J.; Mukamel, S. *Phys. Rev. A* **1990**, *41*, 6485. Yan, Y. J.; Mukamel, S. *J. Chem. Phys*. **1991**, *94*, 179.

(36) Vöhringer, P.; Arnett, D. C.; Westervelt, R. A.; Feldstein, M. J.; Scherer, N. F. *J. Chem. Phys*. **1995**, *102*, 4027.

(37) Nibbering, E. T. J.; Wiersma, D. A.; Duppen, K. *Phys. Rev. Lett*. **1991**, *66*, 2464. Nibbering, E. T. J.; Wiersma, D. A.; Duppen, K. *Phys. Rev. Lett*. **1992**, *68*, 514.

(38) Lyle, P. A.; Kolaczkowski, S. V.; Small, G. J. *J. Phys. Chem*. **1993**, *97*, 6924. Hayes, J. M.; Lyle, P. A.; Small, G. J. *J. Chem. Phys.* **1994**, *98*, 7337.

(39) Hayes, J. M.; Small, G. J. *J. Phys. Chem*. **1986**, *90*, 4928.

(40) Jankowiak, R.; Hayes, J. M.; Small, G. J. *Chem. Rev*. **1993**, *93*, 1471.

(41) Skinner, J. L.; Laird, B. B. *J. Chem. Phys*. **1991**, *94*, 4391. Skinner, J. L.; Laird, B. B. *J. Chem. Phys*. **1991**, *94*, 4405.

(42) Davis, W. B.; Wasielewski, M. R.; Kosloff, R.; Ratner, M. A. *J. Chem. Phys.* **1998**, *102*, 9360.

(43) Kosloff, R.; Ratner, M. A.; Davis, W. B. *J. Chem. Phys*. **1997**, *106*, 7036.

(44) Lindblad, G. *Commun. Math. Phys.* **1976**, *48*, 119.

(45) Toutounji, M.; Kapral, R. *Chem. Phys*. **2001**, *79*, 268.

(46) Silbey, R.; Harris, R. A. *J. Chem. Phys*. **1985**, *80*, 2615. Silbey, R.; Harris, R. A. *J. Phys. Chem*. **1989**, *93*, 7062.